

# Intrinsic Ancillary Ligand Effects in Cationic Zirconium Polymerization Catalysts: Gas-Phase Reactions of $[L_2ZrCH_3]^+$ Cations with Alkenes

David E. Richardson,<sup>\*,†</sup> N. George Alameddin,<sup>†</sup> Matthew F. Ryan,<sup>†</sup>  
Thomas Hayes,<sup>†</sup> John R. Eycler,<sup>†</sup> and Allen R. Siedle<sup>‡</sup>

Contribution from the Department of Chemistry, University of Florida,  
Gainesville, Florida 32611-7200, and 3M Corporate Research Laboratories,  
St. Paul, Minnesota 55144

Received April 29, 1996<sup>⊗</sup>

**Abstract:** Fourier transform ion cyclotron resonance mass spectrometry was used to study ion/molecule reactions of six cationic methyl metallocenes:  $[Cp_2ZrCH_3]^+$  (**1**; Cp =  $\eta^5$ -cyclopentadienyl),  $[(Ind)(Cp)ZrCH_3]^+$  (**2**; Ind =  $\eta^5$ -indenyl),  $[Ind_2ZrCH_3]^+$  (**3**),  $[ansa-(CH_3)_2Si(\eta^5-C_5H_4)_2ZrCH_3]^+$  (**4**),  $[(Flu)_2ZrCH_3]^+$  (**5**; Flu =  $\eta^5$ -fluorenyl), and  $[ansa-(CH_3)_2Si(\eta^5-C_5Me_4)(N-t-C_4H_9)ZrCH_3]^+$  (**6**). Rate constants and product distributions for reactions with dihydrogen and various deuterium-labeled and unlabeled alkenes were determined. The electrophilicity of  $[L_2Zr-CH_3]^+$  ions in the gas phase is strongly dependent on the nature of the ancillary ligands L, with electrophilicity decreasing in the order Cp<sub>2</sub> > Cp,Ind > Ind<sub>2</sub> > Flu<sub>2</sub> for reactions with dihydrogen and 1-alkenes. Silyl-bridging of Cp ligands as in **4** appears to increase the electrophilicity somewhat, and the 10-electron ion **6** also has higher electrophilicity than **1**. In each reaction used to assess electrophilicity, the probable rate determining transition state involves a 4-center/4-electron species in either C–H or H–H activation. In the reaction of ethylene with  $[L_2Zr-CH_3]^+$ , labeling studies show partial-to-complete scrambling of H/D labels before elimination of dihydrogen. Scrambling increases with decreasing electrophilicity of the ion. A model for the intramolecular isotope effect leads to  $k_H/k_D = 2.2$  for the allylic C–H(D) activation step in reaction of **3** with ethylene. Isotopic labeling has shown that the C–H activation of isobutene by  $[L_2Zr-CH_3]^+$  proceeds via allylic activation only. Dimerization and hydrolysis of  $[L_2Zr-CH_3]^+$  is facile in the gas phase, and the products are analogous to known side reactions in solution chemistry. The polymerization activity of electrophilic zirconium polymerization catalysts does not necessarily correlate with the intrinsic electrophilicity of  $[L_2Zr-CH_3]^+$  species as L is varied. The ion pairing tendency of  $[L_2Zr-CH_3]^+$  in solution is a key contributor to the overall propagation rate, and the stability ( $K_{ip}$ ) of the ion pair for a given counterion is expected to decrease as L becomes more electron donating and larger. If the ion pair preequilibrium trends dominate the kinetics, then more active catalysts can be obtained by introducing larger ancillary ligands with electron-donating substituents despite the reduced electrophilicity of the metallocenium ion.

## Introduction

Electrophilic d<sup>0</sup> group 4 metallocenes, such as Cp<sub>2</sub>Zr(CH<sub>3</sub>)<sub>2</sub> (Cp =  $\eta^5$ -cyclopentadienyl), are precursors for alkene polymerization catalysts<sup>1</sup> now entering commercial application.<sup>2</sup> The active species in these catalysts, generally accepted to be the 14-electron cation  $[L_2ZrCH_3]^+$  (L = Cp or related ligands),<sup>3</sup> is formed via reaction of the neutral precursor with cocatalysts such as methylaluminoxane (MAO)<sup>4</sup> and other strong Lewis acids, e.g. B(C<sub>6</sub>F<sub>5</sub>)<sub>3</sub>.<sup>5</sup> In a recent publication,<sup>6</sup> we reported gas-phase ion/molecule reactions of  $[Cp_2ZrCH_3]^+$  (**1**),  $[(Ind)(Cp)ZrCH_3]^+$  (**2**; Ind =  $\eta^5$ -indenyl),  $[Ind_2ZrCH_3]^+$  (**3**),  $[ansa-(CH_3)_2Si(C_5H_4)_2ZrCH_3]^+$  (**4**), and  $[Flu_2ZrCH_3]^+$  (**5**; Flu =  $\eta^5$ -fluorenyl) with dihydrogen and ethylene. It was shown that an *intrinsic* order of electrophilicity for these methylzirconium cations could be determined based on the rates of reactions with

the two substrates. The silyl-bridged complex **4** was shown to be the most electrophilic, and electrophilicity for the L = Cp, Ind, or Flu compounds decreased in the order **1** > **2** > **3** > **5**.

Contrasting the gas-phase results with reported trends for solution polymerization activity as a function of ancillary ligands strongly suggests that polymerization activity is often dominated by factors other than electrophilicity toward monomer insertion. Permethylcyclopentadienyl (Cp\*) and indenyl (Ind) are more electron releasing than Cp itself,<sup>7</sup> yet they can lead to more active catalysts in some cases.<sup>8,9</sup> Studies of alkene polymerization by substituted bis(indenyl)zirconium(IV) catalysts show that electron-withdrawing substituents (e.g., X = Cl, F) lead to reduced activity compared to X = H.<sup>10,11</sup> In the latter examples, electronic effects are assumed to be important factors since the site of substitution is remote from the metal center. Thus, increased electrophilicity due to the nature of the ancillary ligands does not translate into higher polymerization activity, and we have suggested that the overall solution polymerization

<sup>†</sup> University of Florida.

<sup>‡</sup> 3M Laboratories.

<sup>⊗</sup> Abstract published in *Advance ACS Abstracts*, November 1, 1996.

(1) Mohring, P. C.; Coville, N. J. *J. Organomet. Chem.* **1994**, *479*, 1.

(2) Thayer, A. M. *Chem. Eng. News* **1995**, *73*(37), 15–20.

(3) Jordan, R. F. *Adv. Organomet. Chem.* **1991**, *32*, 325.

(4) Sinn, H.; Kaminsky, W.; Vollmer, H.; Woldt, R. *Angew. Chem.* **1980**, *92*, 396.

(5) Yang, X.; Stern, C. L.; Marks, T. J. *J. Am. Chem. Soc.* **1994**, *116*, 10015 and references therein.

(6) Alameddin, N. G.; Ryan, M. F.; Eycler, J. R.; Siedle, A. R.; Richardson, D. E. *Organometallics* **1995**, *14*, 5005.

(7) Gassman, P. G.; Winter, C. H. *J. Am. Chem. Soc.* **1988**, *110*, 6130.

(8) Resconi, L.; Piemontesi, F.; Franciscano, G.; Abis, L.; Fiorani, T. *J. Am. Chem. Soc.* **1992**, *114*, 1025.

(9) Giannetti, E.; Nicoletti, G. M.; Mazzocchi, R. *J. Polym. Sci., Polym. Chem. Ed.* **1985**, *23*, 2117.

(10) Lee, I.-K.; Gauthier, W. J.; Ball, J. M.; Iyengar, B.; Collins, S. *Organometallics* **1992**, *11*, 2115.

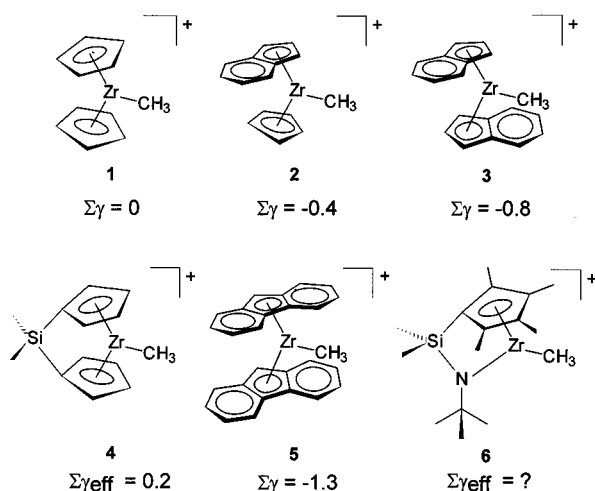
(11) Piccolrovazzi, N.; Pino, P.; Consiglio, G.; Sironi, A.; Moert, M. *Organometallics* **1990**, *9*, 3098.

activity can be dominated by the strength of ion pairing and rates of termination steps in these particular systems.

As shown by recent quantitative studies, substantial ion pairing must be overcome before a monomer can be activated and inserted.<sup>12</sup> The tendency to ion pair is dependent on many factors, including the accessibility of the metal center in the cation (steric effects), the Lewis basicity of the anion, solvation energetics, and the charge density at the metal as it is affected by ancillary ligands. Thus, relative to Cp itself, electron-donating ligands such as Ind can lead to a favorable balance of lower electrophilicity (toward a substrate) compensated by a lower ion pairing because of lessened charge density and increased steric crowding at the metal.

Our focus in studying the gas-phase reactivity of modified metallocene catalysts has been on the *electronic* factors that will influence both electrophilicity toward substrates and the tendency of the cationic metallocene to ion pair with counterions. We have found that the  $\gamma$  parametrization<sup>13–17</sup> of Cp derivatives is a useful way to correlate the intrinsic, gas-phase reactivity of group 4 methylmetallocenium ions with various ancillary ligands. The  $\gamma$  parameters are based on the ionization free energies for the reaction  $LL'M \rightleftharpoons LL'M^+ + e^-$ , where L and L' are Cp derivatives and M is either Fe, Ru, or Ni. The gas-phase electron-transfer equilibrium technique is used to determine the ionization free energies. By assigning ligand parameters  $\gamma_L$  to Cp ( $\gamma_L = 0$ ) and Cp\* ( $\gamma_L = -1$ ), a set of parameters for a variety of Cp derivatives can be derived. It is assumed in the derivation of the parameters that ligand effects are additive for L and L'. Negative values of  $\gamma_L$  indicate a tendency to decrease the metallocene ionization energy relative to Cp while derivatives with positive  $\gamma_L$  values increase the ionization energy.

Some of the cations examined in the present study are shown below with their  $\Sigma\gamma$  values. In the case of **4**, only an effective  $\Sigma\gamma$  value can be deduced from reactivity studies.<sup>6</sup>



In the initial studies of the gas-phase reactions of **1**,<sup>18–20</sup> it was observed that ethylene insertion is followed by intramo-

lecular C–H activation to eliminate H<sub>2</sub>. Extensive scrambling of H and D was noted when CD<sub>2</sub>CD<sub>2</sub> was allowed to react with **1**, leading to elimination of H<sub>2</sub>, HD, and D<sub>2</sub>. With larger alkenes having no  $\beta$ -hydrogen such as isobutene, direct C–H activation of the substrate was observed in reactions of [Cp<sub>2</sub>ZrCD<sub>3</sub>]<sup>+</sup> (only CD<sub>3</sub>H is eliminated). The site of C–H activation was not determined, but this question has been resolved in the present work.

The ancillary Cp/amide chelating ligand of compound **6** has recently been used in group 4 polymerization catalysts.<sup>21</sup> A dimethyl precursor to **6** has been synthesized by Peterson and co-workers.<sup>22</sup> The high reactivity of catalysts with this type of ligand is assumed to be related to the increased electrophilicity of the metal center in a formally 10-electron complex.

In this article, we present data for the reactions of **1–6** with deuterium-labeled and unlabeled dihydrogen and alkenes. One goal of the study was to assess the effect of the ancillary ligands on the reaction kinetics and extent of label scrambling in reactive intermediates. Labeled substrates are used to identify sites of C–H activation, and a kinetic isotope effect for intramolecular C–H(D) activation has been determined. The relative electrophilicity of **6** has been determined for comparison with the trends observed for **1–5**. The kinetics of zirconium dimer formation were also examined since these dimers may be critical in controlling catalytic activity.<sup>23</sup> Finally, an overall picture of the relationship between gas-phase and solution reactivity is presented that incorporates kinetic and mechanistic results from this study.

## Results and Discussion

Assignment of product structures from ion/molecule reactions is largely based on fragmentation analysis, empirical formulas, and chemical precedent. In the results below, no particular structure is initially assumed except the bent metallocene fragment ion, [L<sub>2</sub>Zr]<sup>+</sup>. Previous collisionally activated dissociation (CAD) of **1** has shown that the [Cp<sub>2</sub>Zr]<sup>+</sup> unit remains intact, and no evidence that the other ancillary ligands participate in the reactions has been found. Products will therefore be written L<sub>2</sub>ZrC<sub>x</sub>H<sub>y</sub>O<sub>z</sub> (with D and <sup>13</sup>C as appropriate). Neutral products are assumed to be the most stable molecules with the correct molecular formula.

For the discussion of reaction pathways, structural details of the ions are based primarily on analogies to the chemistry of **1** reported previously.<sup>18–20</sup> Mechanistic schemes and rationales thus follow this assumption although extensive fragmentation studies have not been done as in the original work. Scheme 1 summarizes the assumed mechanisms of various reactions studied in this work (for L = Cp) and the expected product structures.

(18) Christ, C. S.; Eyler, J. R.; Richardson, D. E. *J. Am. Chem. Soc.* **1988**, *110*, 4038.

(19) Christ, C. S.; Eyler, J. R.; Richardson, D. E. *J. Am. Chem. Soc.* **1990**, *112*, 596.

(20) Christ, C. S.; Eyler, J. R.; Richardson, D. E. *J. Am. Chem. Soc.* **1990**, *112*, 4778.

(21) (a) Canich, J. M. European Patent Application EP-420-436-A1, 1991. (b) Canich, J. M. U.S. Patent Application 5,026,798, 1991. (c) Canich, J. M.; Hlatky, G. G.; Turner, H. W. PCT Application WO92-00333, 1992. (d) Stevens, J. C.; Timmers, F. J.; Wilson, D. R.; Schmidt, G. F.; Nickias, P. N.; Rosen, R. K.; Knight, G. W.; Lai, S. European Patent Application EP-416-815-A2, 1991.

(22) (a) Carpenetti, D. W.; Kloppenburg, L.; Kupec, J. T.; Petersen, J. L. *Organometallics* **1996**, *15*, 1572–1581. (b) Kloppenburg, L.; Petersen, J. L. *Organometallics* **1996**, *15*, 7–9.

(23) (a) Boehmann, M.; Lancaster, S. J. *Angew. Chem., Int. Ed. Engl.* **1994**, *33*, 1634. (b) Stehling, U.; Diebold, J.; Kirsten, R.; Röhl, W.; Brintzinger, H.-H.; Jüngling, S.; Mülhaupt, R.; Langhauser, F. *Organometallics* **1994**, *13*, 964.

(12) (a) Deck, P. A.; Marks, T. J. *J. Am. Chem. Soc.* **1995**, *117*, 6128. (b) Siedle, A. R.; Newmark, R. A. *J. Organomet. Chem.* **1995**, *497*, 119.

(13) Richardson, D. E. In *Organometallic Ion Chemistry*; Freiser, B. S., Ed.; Kluwer Academic Publishers: Dordrecht, 1996; Ch. 8.

(14) Richardson, D. E.; Ryan, M. F.; Khan, Md, N. I.; Maxwell, K. A. *J. Am. Chem. Soc.* **1992**, *114*, 10482.

(15) Ryan, M. F.; Eyler, J. R.; Richardson, D. E. *J. Am. Chem. Soc.* **1992**, *114*, 8611.

(16) Ryan, M. F.; Richardson, D. E.; Lichtenberger, D. L.; Gruhn, N. *Organometallics* **1994**, *13*, 1190.

(17) Ryan, M. F.; Siedle, A. R.; Burk, M. J.; Richardson, D. E. *Organometallics* **1992**, *11*, 4231.

## Scheme 1

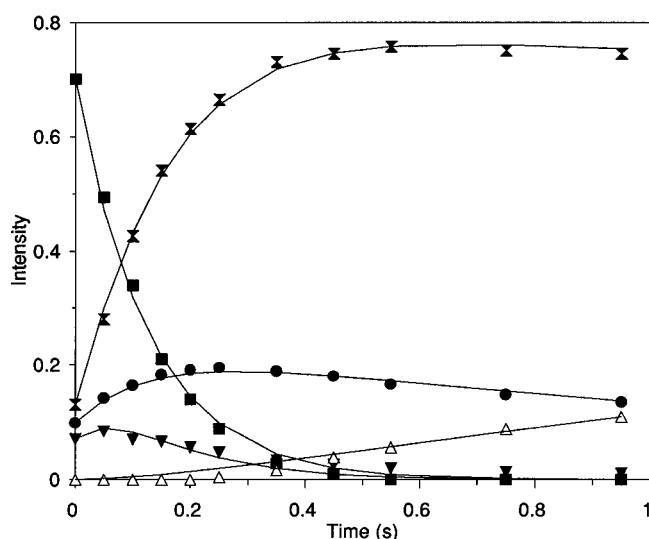
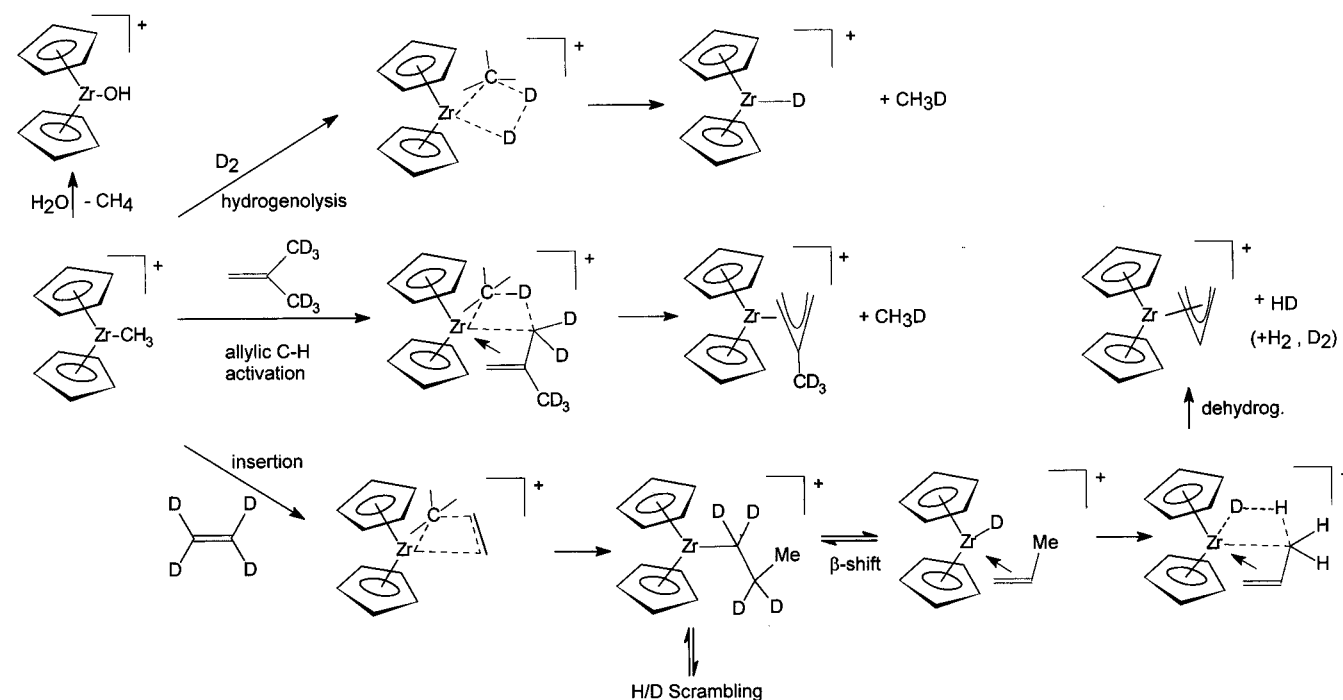
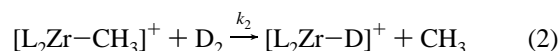
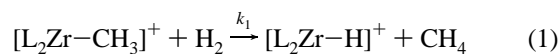


**Figure 1.** Fit of kinetic model to experimental ion intensities for the reaction of  $[\text{Cp}_2\text{Zr}^{13}\text{CH}_3]^+$  with unlabeled ethylene. Normalized experimental ion intensities:  $\blacksquare$ ,  $[\text{Cp}_2\text{Zr}^{13}\text{CH}_3]^+$ ;  $\bullet$ ,  $[\text{Cp}_2\text{ZrC}_3\text{H}_5]^+$ ;  $\triangle$  and stacked triangles,  $\text{Zr}_2$  dimers (all types);  $\blacktriangledown$ ,  $[\text{Cp}_2\text{ZrOH}]^+$  (from reaction with background water). Lines are results of model fit.

**Reactions and Rate Constants.** The rate constants for various reaction pathways of interest were obtained by fitting

ion intensity data to a kinetic scheme containing the reactions and products observed in each system (see Experimental Section). An example of a kinetic fit of an ion intensity vs time plot is shown in Figure 1. The rate constants derived from the data fits for the primary reactions in this study (eqs 1–8 below) are collected in Table 1. Some of the rate constants are plotted against  $\Sigma\gamma$  values in Figure 2. Reactions are grouped and discussed below.

**(a)  $\text{H}_2/\text{D}_2$  Reactions.** The reaction with  $\text{H}_2$  ( $\text{D}_2$ ) results in exclusive formation of the metal–hydride (metal–deuteride) with loss of  $\text{CH}_4$  ( $\text{CH}_3\text{D}$ ) (eqs 1 and 2). The rate constants for eq 1 as a function of L were reported previously and are shown in Figure 2.<sup>6</sup>



Kinetic isotope effects (KIE,  $k_1/k_2$ ) are calculated from these two hydrogenolysis reactions:  $2.4 \pm 1.3$  (1),  $1.3 \pm 1.7$  (2),  $3.7 \pm 5.0$  (3),  $1.2 \pm 0.2$  (4). The statistics on these reactions were not sufficiently good to identify a trend in the H/D isotope effect as a function of the ancillary ligand.

**(b)  $\text{C}_2\text{H}_4/\text{C}_2\text{D}_4$  Reactions.** The reactions of  $[\text{L}_2\text{Zr}-\text{CH}_3]^+$  with  $\text{C}_2\text{H}_4$  yield the dehydrogenated metal–allyl product

**Table 1.** Rate Constants for the Reaction of 1–4 with  $\text{H}_2$ ,  $\text{D}_2$ ,  $\text{C}_2\text{H}_4$ ,  $\text{C}_2\text{D}_4$ ,  $\text{C}_3\text{H}_6$ ,  $\text{C}_4\text{H}_8$ ,  $\text{C}_4\text{H}_6\text{D}_2$ , and  $\text{C}_4\text{H}_2\text{D}_6$

rate constant <sup>a</sup>	compd			
	1	2	3	4
$k_1$	$(3.9 \pm 1.2) \times 10^{10}$	$(2.6 \pm 0.7) \times 10^8$	$(4.8 \pm 4.4) \times 10^7$	$(6.9 \pm 0.3) \times 10^{10}$
$k_2$	$(1.6 \pm 0.7) \times 10^{10}$	$(2.0 \pm 2.5) \times 10^8$	$1.3 \times 10^7$ <sup>b</sup>	$(5.6 \pm 0.7) \times 10^{10}$
$k_3$	$(3.4 \pm 0.9) \times 10^{10}$	$(2.1 \pm 1.4) \times 10^9$	$(3.5 \pm 0.4) \times 10^8$	$(9.6 \pm 1.8) \times 10^{10}$
$k_4$	$(3.5 \pm 1.1) \times 10^{10}$	$(1.3 \pm 0.5) \times 10^9$	$(2.8 \pm 1.3) \times 10^8$	$(6.1 \pm 2.9) \times 10^{10}$
$k_5$	$(2.8 \pm 0.3) \times 10^{10}$	$(5.4 \pm 2.6) \times 10^8$	$(9.2 \pm 3.6) \times 10^7$	$(3.1 \pm 1.3) \times 10^{10}$
$k_6$	$(1.1 \pm 0.7) \times 10^{10}$	$(2.2 \pm 0.8) \times 10^8$	$(4.8 \pm 3.0) \times 10^7$	$(2.8 \pm 0.3) \times 10^{10}$
$k_7$	(not measured) <sup>c</sup>	$(1.6 \pm 0.3) \times 10^8$	$3.8 \times 10^7$ <sup>*</sup>	$(9.8 \pm 2.9) \times 10^9$
$k_8$	$(8.0 \pm 2.5) \times 10^9$	$(\sim 10^8)$ <sup>c</sup>	$5.3 \times 10^7$	$(6.0 \pm 1.2) \times 10^9$

<sup>a</sup> All rate constants in units of  $\text{M}^{-1} \text{s}^{-1}$ . To convert to units of  $\text{cm}^3 \text{s}^{-1}$ , divide by  $6.022 \times 10^{20}$ . <sup>b</sup> Due to poor signal to noise, only one measurement was used. <sup>c</sup> Measurements not reproducible.

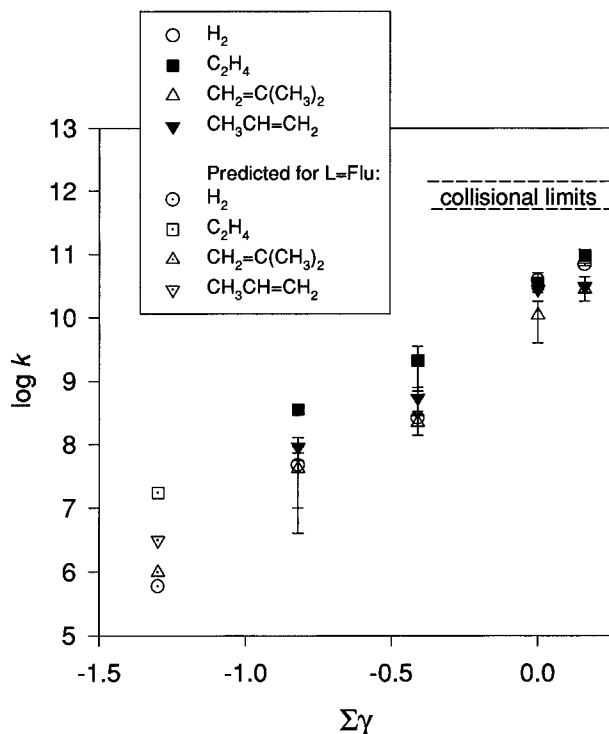
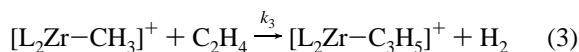


**Figure 2.** Plot of rate constants for reactions of **1–4** with substrates indicated in the legend. For complex **4**, rate constants predicted by a fit of other data are shown.

reported previously<sup>18,19</sup> (eq 3 and Scheme 1):



The dependence of  $k_3$  on L is plotted in Figure 2.

The rate constant for reaction of **6** with ethylene is  $8.0 \pm 1.5 \times 10^{10} \text{ M}^{-1} \text{ s}^{-1}$ , giving a  $\Sigma\gamma_{\text{eff}} \approx 0.15$ , which is comparable to that of the related *ansa* complex **4**. Increased electrophilicity expected for replacement of Cp by an amide in **6** (producing a 10-electron complex) is evidently compensated by permethylation of the remaining Cp (each methyl group contributes  $-0.2$  to  $\gamma$ ).<sup>17</sup> The fit of kinetic data for this reaction was complicated by the presence of an unreactive ion at the same mass/charge value as the reactive ion **6**. This unreactive ion is  $\sim 30\%$  of the total initial ion population at that mass and is presumably a rearrangement product of **6** produced following electron impact on the neutral precursor. The fit of the kinetic model, which includes the unreactive fraction, is shown in Figure 3.

Reaction with  $\text{C}_2\text{D}_4$  (eq 4) gives three different products. If all seven hydrogenic atoms are scrambled statistically before



elimination and the elimination process has no isotope effect, then the predicted product distribution is 14.3%  $\text{H}_2$ , 57.1% HD, and 28.6%  $\text{D}_2$ . The experimentally observed distributions are given in Table 2, and an average rate constant  $k_4$  is given in Table 1.

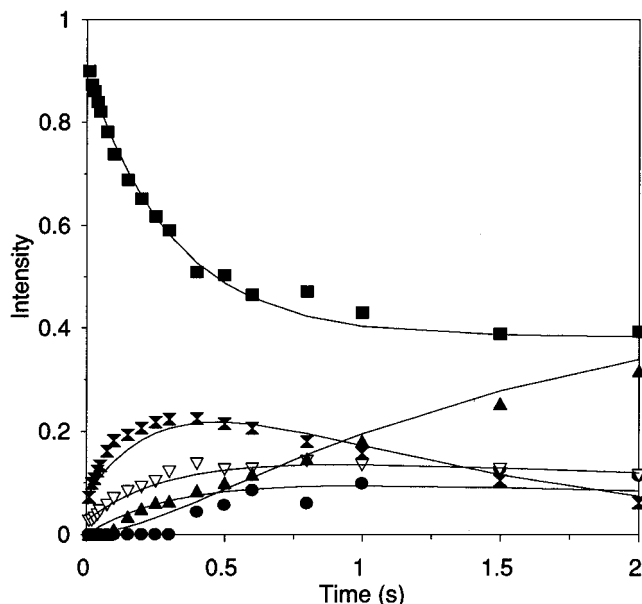


**Figure 3.** Fit of kinetic model to experimental ion intensities for the reaction of **6** with ethylene. Normalized experimental ion intensities:  $\blacksquare$ ,  $[\text{L}_2\text{ZrCH}_3]^+$  and unreactive ion at the same  $m/z$  value;  $\nabla$ ,  $[\text{L}_2\text{ZrC}_3\text{H}_5]^+$ ;  $\blacktriangle$ ,  $\text{Zr}_2$  dimers (all types);  $\bullet$ ,  $[\text{L}_2\text{ZrOH}]^+$  (from reaction with background water); stacked triangles,  $([\text{L}_2\text{ZrCH}_3]^+ - \text{CH}_4)$  (loss of methane from the parent ion). The kinetic model (lines) includes an unreactive ion of the same mass as **6**.

**Table 2.** Product Distributions<sup>a</sup> for  $[\text{L}_2\text{Zr}-\text{CH}_3]^+ + \text{C}_2\text{D}_4 \rightarrow [\text{L}_2\text{Zr}-\text{C}_3\text{H}_{3-x}\text{D}_{2+x}]^+ + \text{H}_x\text{D}_{2-x}$

elim neutral	x	statistical distribution <sup>b</sup>	compd			
			1 (calc <sup>c</sup> )	2 (calc <sup>c</sup> )	3 (calc <sup>c</sup> )	4
$\text{D}_2$	0	28.6	16 (17)	14 (15)	19 (18)	13
HD	1	57.1	64 (60)	63 (60)	58 (60)	74
$\text{H}_2$	2	14.3	20 (23)	23 (24)	24 (22)	13

<sup>a</sup> All values expressed as percent. Estimated experimental errors  $\pm 2\%$ . <sup>b</sup> Based on the equal participation of the three hydrogens and the four deuteria. <sup>c</sup> From equations in the text with  $k_H/k_D = 2.3$  (**1**), 2.7 (**2**), 2.2 (**3**).

It is clear from the results in Table 2 that the product distributions for the elimination reactions of eq 4 are *not* indicative of purely statistical scrambling before elimination. The fraction of HD eliminated decreases from 74% to 58% in the order  $4 > 1 \approx 2 > 3$ , which is the order of decreasing electrophilicity. If no scrambling occurs, 100% HD elimination is expected since the direct reaction mechanism (Scheme 1) eliminates one hydrogen from the methylzirconocenium ion with one from the substrate. However, scrambling of labels before elimination, as shown in Scheme 1, lowers the HD fraction in the products. Evidently, some combination of electronic and steric effects reduces the rate of scrambling relative to direct elimination of HD in the order noted.

Although the HD elimination is nearly statistical in the reaction of **1–3** with  $\text{C}_2\text{D}_4$ , the fraction of  $\text{D}_2$  is low, suggesting an intramolecular kinetic isotope effect (IKIE) in the elimination reaction of eq 4. The following model can be used to estimate the IKIE.

We assume that H and D can scramble to every position on the Zr-propyl intermediate formed by insertion of ethylene into the Zr–Me bond (Scheme 1). This scrambling may occur via a variety of mechanisms once the propyl complex is formed. We assume that the equilibrium isotope effect accompanying the scrambling is negligible. Elimination of  $\text{D}_2$ ,  $\text{H}_2$ , and HD is assumed to occur with a IKIE defined primarily by the rates of C–H vs C–D activation at the *allylic* hydrogen of the Zr–

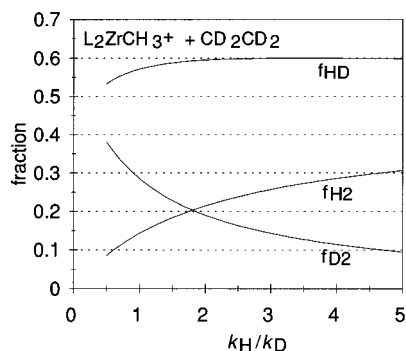
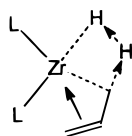


**Figure 4.** Plot of the model fractional abundances of H<sub>2</sub>, D<sub>2</sub>, and HD as a function of the kinetic isotope ratio for the reaction of eq 4 in text. The curves are calculated by using the equations for *f* in the text.

hydride–propylene intermediate:



In other words, the model assumes that the probability of forming Zr–H and Zr–D depends only on the numbers of H and D in the reactants (4 D and 3 H in eq 4) and that the IKIE depends only on whether H or D is migrating from the allylic carbon to the metal-bound hydride prior to elimination. (Support for the assumption of allylic activation of bound propylene is given in the next section.) With these assumptions, the following equations can be derived for the fractions of D<sub>2</sub>, H<sub>2</sub>, and HD eliminated:

$$f_{\text{H}_2} = \frac{n_{\text{H}}}{n_{\text{H}} + n_{\text{D}}} \left( \frac{1}{R\alpha} + 1 \right)^{-1}$$

$$f_{\text{D}_2} = \frac{n_{\text{D}}}{n_{\text{H}} + n_{\text{D}}} \left( \frac{R}{\beta} + 1 \right)^{-1}$$

$$f_{\text{HD}} = \frac{n_{\text{H}}}{n_{\text{H}} + n_{\text{D}}} (R\alpha + 1)^{-1} + \frac{n_{\text{D}}}{n_{\text{H}} + n_{\text{D}}} \left( \frac{1}{R\beta} + 1 \right)^{-1}$$

where

$$\alpha = \frac{n_{\text{H}} - 1}{n_{\text{D}}} \quad \beta = \frac{n_{\text{D}} - 1}{n_{\text{H}}} \quad R = \frac{k_{\text{H}}}{k_{\text{D}}}$$

and  $n_{\text{H}}$  and  $n_{\text{D}}$  are the numbers of H and D subject to scrambling, respectively. The kinetic ratio  $k_{\text{H}}/k_{\text{D}}$  is expected to be  $> 1$  since C–H activation is favored over C–D activation. A plot of  $f_{\text{H}_2}$ ,  $f_{\text{D}_2}$ , and  $f_{\text{HD}}$  vs  $k_{\text{H}}/k_{\text{D}}$  is shown in Figure 4. If  $k_{\text{H}}/k_{\text{D}} = 1$ , then the purely statistical fractions given earlier are predicted, but when  $k_{\text{H}}/k_{\text{D}} > 1$ , the amount of D<sub>2</sub> eliminated begins to drop from 28.6%. As  $k_{\text{H}}/k_{\text{D}}$  gets very large, the percent of HD does not go to zero since it can still be eliminated from the L<sub>2</sub>ZrD–(propylene)<sup>+</sup> complex.

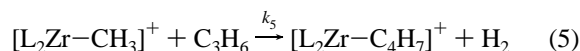
Referring to Table 2, the data for **1**, **2**, and **3** are best fit (least squared errors) with  $k_{\text{H}}/k_{\text{D}} = 2.3$ , 2.7, and 2.2, respectively, and the observed fractions are within experimental error of the calculated values. The quality of the fit suggests that a more sophisticated model for the IKIE is not needed. The values of  $k_{\text{H}}/k_{\text{D}}$  are comparable to the primary KIE for H migration in electrophilic permethylscandocene alkyl complexes.<sup>24</sup> The

(24) Burger, B. J.; Thompson, M. E.; Cotter, W. D.; Bercaw, J. E. *J. Am. Chem. Soc.* **1990**, *112*, 1566.

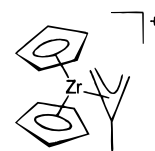
observed distribution for the highly electrophilic **4** is not fit well since the maximum  $f_{\text{HD}}$  in the model is  $\sim 60\%$  (compare to 74% observed). This observation confirms that H/D scrambling in the L<sub>2</sub>Zr–propyl intermediate is incomplete before elimination for this highly reactive ion.

With regard to the mechanism of H/D scrambling in the L<sub>2</sub>–Zr–propyl complex, it is noted that recent work by Baird and co-workers<sup>25</sup> supports the participation of carbocations in the polymerization of styrene by Cp\*TiMe<sub>2</sub><sup>+</sup>. If energetically accessible in the present Zr ions, such intermediates would scramble H and D labels as commonly observed in the mass spectrometric analysis of labeled alkyl hydrocarbons. Alternatively, repetitive intramolecular insertion/ $\beta$ -H(D) migration (deinsertion) steps can lead to scrambling.

**(c) Propylene Reactions.** The reaction with propylene yields a dehydrogenated product following insertion of the propylene into the metal–methyl bond (eq 5) forming, presumably, the methylallyl complex:

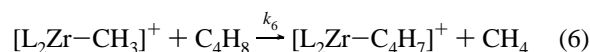


The assumed structure of the product ion is that resulting from Markovnikov addition of propylene:

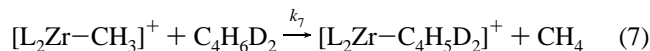


The trends in the rates of eq 5 as a function of ancillary ligand parallel those reported previously for ethylene, i.e., **4**  $>$  **1**  $>$  **2**  $>$  **3**, and the rate constants are plotted as a function of  $\Sigma\gamma$  in Figure 2.

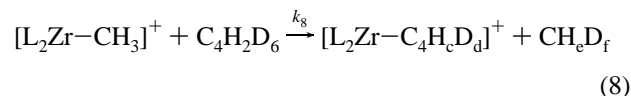
**(d) Isobutene C–H Activation Reactions.** The reaction with isobutene gives the methyl allyl (eq 6) after loss of methane ( $\sigma$ -bond metathesis—see Scheme 1):



The values of  $k_6$  in Table 1 clearly follow the same trend seen for reactions with dihydrogen, ethylene and propylene (Figure 2). In the reaction with deuterated isobutenes, the d<sub>2</sub> analog (D<sub>2</sub>C=C(CH<sub>3</sub>)<sub>2</sub>) gives the same neutral product as the non-deuterated isobutene (eq 7):



This is consistent with an *allylic* activation mechanism. Allylic activation is known for other gas-phase<sup>26</sup> and condensed-phase<sup>27</sup> C–H activation reactions. Similarly, the vinylic hydrogens in the d<sub>6</sub> analog (H<sub>2</sub>C=C(CD<sub>3</sub>)<sub>2</sub>) are not involved in the reaction. In this case, however, a variety of products are produced (eq 8):



The scrambling here appears to be the result of initial insertion followed by  $\beta$ -methyl shift and C–H activation, eliminating

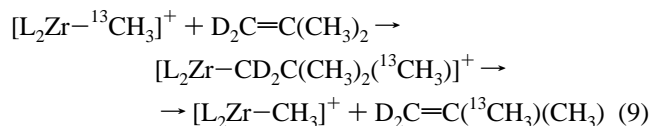
(25) Wang, Q.; Quyoum, R.; Gillis, D. J.; Tudoret, M.-J.; Jeremic, D.; Hunter, B. K.; Baird, M. C. *Organometallics* **1996**, *15*, 693.

(26) Jacobsen, D. B.; Frieser, B. S. *J. Am. Chem. Soc.* **1985**, *107*, 5876.

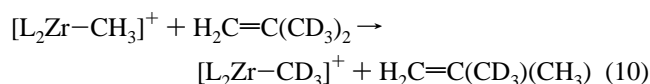
(27) Eshuis, J. J. W.; Tan, Y. Y.; Meetsma, A.; Teuben, J. H. *Organometallics* **1992**, *11*, 362 and references therein.

methane (next section). This mechanism could in principle be tested by the predicted absence of CH<sub>2</sub>D<sub>2</sub> elimination in the products. Unfortunately, the low yield from this reaction and overlapping isotopic distributions makes it difficult to compute a meaningful product distribution.

(e) **Insertion of Isobutene.** For compounds **1** and **4**, we used <sup>13</sup>C-labeled parent complexes to follow a reaction pathway for isobutene in which a facile insertion/ $\beta$ -Me elimination process involving an intermediate neopentyl complex (not observed) leads to methyl scrambling as shown below (eq 9):



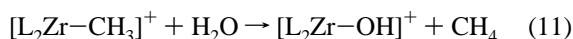
The same exchange reaction can be followed for the reaction of **1–4** with H<sub>2</sub>C=C(CD<sub>3</sub>)<sub>2</sub>, shown below:



The product, [L<sub>2</sub>Zr–CD<sub>3</sub>]<sup>+</sup>, goes on to react to yield CD<sub>4</sub> as the only product (by analogy to eq 7). No apparent H/D scrambling is noted for eq 10; only intact methyl groups are exchanged. These degenerate pathways do not affect the kinetics for eqs 6–8 since they are unseen in the absence of labels.

The extensive scrambling observed in the reaction of eq 8 is therefore assigned as the product of wholly intramolecular insertion/ $\beta$ -methyl shift/C–H activation.

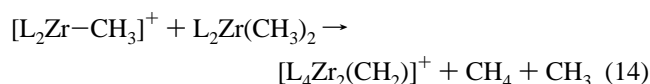
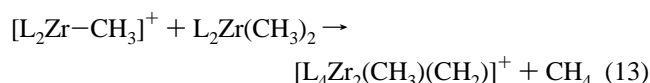
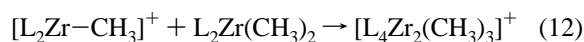
(f) **Hydrolysis Reactions.** Given the difficulty of removing all traces of water from the vacuum chamber and the extremely oxophilic nature of these complexes, it is not surprising that the reaction with water is facile (eq 11 and Scheme 1).



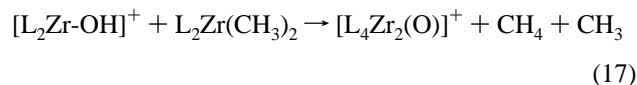
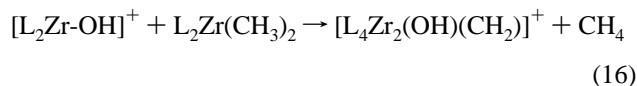
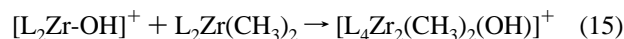
If the background pressure is all water in our instrument, then the rates for eq 11 were near Langevin (collisional) for all ancillary ligand sets. Reactions with water were included in the kinetic schemes used to fit the ion intensity vs time data.

**Dimerization Reactions.** Dimers are formed due to the reaction of various reactant and product zirconocenium ions with neutral L<sub>2</sub>Zr(CH<sub>3</sub>)<sub>2</sub> and are observed as (at most) five distinct envelopes of peaks. The loss of mononuclear Zr-containing ions to dimerization is explicitly included in the kinetic modeling used to obtain the rate constants in Table 1. However, it was found that the rates of various dimer-forming reactions were rapid and no regular dependence on the ancillary ligands was observed.

Dimers were formed via a variety of reactions. For example, the cations **1–6** react with their corresponding neutrals, L<sub>2</sub>Zr(CH<sub>3</sub>)<sub>2</sub>, to form adducts with and without neutral elimination (e.g., eqs 12–14).

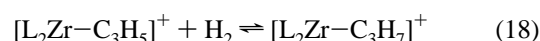


The hydroxide complex formed by the reaction of eq 11 also undergoes facile dimer formation via analogous reactions (eqs 15–17).



Dimer formation was included in the kinetic schemes.

**Reactions of Allyl Product Ions with Dihydrogen.** In principle, all Zr–allyl product ions produced (e.g., via eqs 3–8) can react with dihydrogen reversibly to form an unobserved Zr–alkyl ion (eq 18).



The rate of this reaction will depend on the barriers separating the thermalized allyl complex from the alkyl complex and thus can provide evidence concerning the potential surface that controls the reactivity (vide infra). Under thermal conditions, [L<sub>2</sub>Zr–C<sub>3</sub>H<sub>5</sub>]<sup>+</sup> formed by eq 3 is unreactive with dihydrogen (deuterium labeling was used to follow possible reaction and scrambling of the propyl intermediate prior to elimination of dihydrogen). When [L<sub>2</sub>Zr–C<sub>3</sub>H<sub>5</sub>]<sup>+</sup> was translationally activated in the presence of dihydrogen, only previously observed CAD product ions were observed. It is concluded that the [L<sub>2</sub>Zr–C<sub>3</sub>H<sub>5</sub>]<sup>+</sup> product energy is substantially below that of the transition state for the forward reaction in eq 18.

**Alkylated Cyclopentadienyl complexes and the fluorenyl complex (5).** A number of other L<sub>2</sub>Zr(CH<sub>3</sub>)<sub>2</sub> precursors were studied in an attempt to characterize additional ancillary ligands. However, they did not give useful kinetic results due to intramolecular reaction or very slow reaction rates as described below.

Alkylated ligands studied include L = *t*-BuCp, (TMS)<sub>2</sub>Cp (TMS = trimethylsilane), and Cp\* (Cp\* = pentamethylcyclopentadienyl). These complexes either fail to produce the desirable parent cation [L<sub>2</sub>Zr–CH<sub>3</sub>]<sup>+</sup> or the parent cation rapidly decomposes in the ion trap eliminating methane. The mechanism of the intramolecular reaction involves the activation of one of the Cp–alkyl C–H bonds and elimination of methane, as shown for the decamethyl complex in Scheme 2.

In complexes with L = Flu (Flu = fluorenyl) or CH<sub>3</sub>-Flu, no hydrocarbon reactions were seen because the rate of reaction was slower than the time scale of the experiment dictated by dimerization reactions or ion loss from the trap. Predicted rates for four reactions with L=Flu are shown in Figure 2 based on the best fit lines to the data for **1–4**.

**Relationship of Intrinsic Ancillary Ligand Effects to Solution Reactivity for Metallocene Catalysts.** As shown conclusively above, the order of reactivity for [L<sub>2</sub>Zr–CH<sub>3</sub>]<sup>+</sup> ions in the gas phase follows a predictable trend for nonbridging Cp derivatives as ancillary ligands. However, decreasing electrophilicity of the [L<sub>2</sub>Zr–CH<sub>3</sub>]<sup>+</sup> reactant does not necessarily lead to decreased polymerization activity in solution; indeed, electron-donating Cp derivatives often lead to increased activity while electron-withdrawing substituents tend to decrease activity.<sup>1,7–10</sup> This lack of correlation clearly results from the complexity of the actual catalytic reaction, where solvent, counterions, and the relative rates of initiation, propagation,

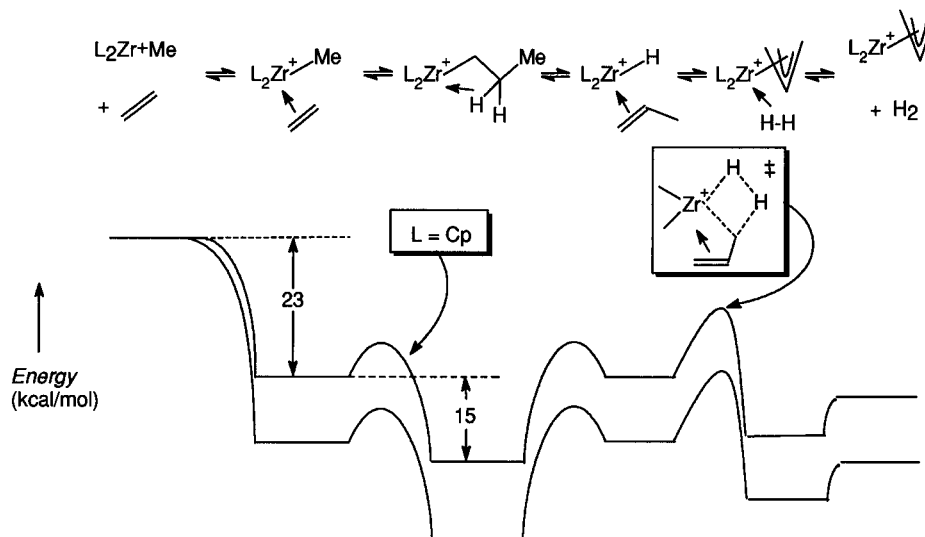
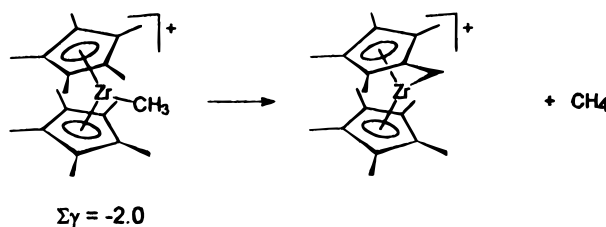


**Figure 5.** Qualitative potential surface for the reaction in eq 3 in the text. The upper surface is for  $L = \text{Cp}$ , while the lower surface represents the qualitative effect of increasing the electrophilicity of the complex via modification of ancillary ligands.

### Scheme 2



termination, and chain transfer can have profound effect on overall activity.

In this section, we attempt to put the above ideas, which are widely appreciated,<sup>1</sup> on a firmer basis. The gas-phase data provide a fundamental view of  $[\text{L}_2\text{Zr}-\text{CH}_3]^+$  reactivity that can be incorporated into a detailed model for polymerization activity in solution. The intrinsic reactivity of  $[\text{L}_2\text{Zr}-\text{CH}_3]^+$  species as probed in gas-phase experiments will be described by a potential energy surface that can reflect the ancillary ligand effects on the relative energies of key intermediates and transition states. Solvation and ion pairing will then be introduced to describe the changes in the reaction surfaces in solution. Finally, the overall kinetics of chain growth in a catalyst will be modeled and related to the energy surfaces described.

In considering the use of the gas-phase results to clarify mechanistic issues in the condensed-phase reactivity of these ions, it is helpful to remember that *electrophilicity* refers to the relative rates of reactions and is not a direct measure of ligand binding tendencies of the metal center. However, ligand binding energies (i.e., as affected by the Lewis acidity of the metal) and transition state energies can follow the same trends when formation of the transition state from separated reactants is essentially the binding of a substrate ligand to the metal in the activated complex.

The gas-phase data provide an intrinsic order of electrophilicity as a function of the ancillary ligand set (Figure 2). It is not surprising that all reactions studied follow the same general trend  $4 \approx 6 > 1 > 2 > 3 > 5$ , since each reaction has a rate-determining step that is controlled by a 4-center/4-electron transition state (i.e., H-H or C-H activation). Potential surfaces that rationalize ancillary ligand effects on the gas-phase reactions with ethylene are shown in Figure 5. The top surface represents the reaction profile for  $L = \text{Cp}$ , and some theoretical

values for the formation of intermediates are shown. Binding of ethylene to the 14-electron cation  $[\text{L}_2\text{Zr}-\text{CH}_3]^+$  is predicted to be exothermic by  $-23$  kcal/mol, and insertion followed by formation of a  $\beta$ -agostic interaction releases an estimated additional  $-15$  kcal/mol (both values from density functional theory (DFT)<sup>28</sup>). The insertion process itself is predicted to have a small or nonexistent barrier by DFT<sup>28</sup> and *ab initio* calculations.<sup>29</sup> The  $\beta$ -H shift to form bound propylene is followed by dihydrogen elimination as the rate-determining step (Scheme 1). The energy of the zirconocenium allyl product ion is not known from *ab initio* results, but we have carried out semiempirical calculations (ZINDO95<sup>30</sup>) that suggest that the total energy of the addition-elimination reaction is about half the energy of initial ethylene insertion (or  $\sim 20$  kcal/mol). The absence of thermal back reaction of  $\text{H}_2$  with the  $[\text{L}_2\text{ZrC}_3\text{H}_5]^+$  product ion indicates that a kinetic barrier (indicated by ‡ in Figure 5) is present at the dehydrogenation step. Although the transition state shown in Figure 5 is below the reactant energy, the overall reaction is still below 100% efficient (i.e., collision limited) due to the tightness of the forward reaction transition state relative to that of the back reaction (dissociation to reactants).

The qualitative effect of increasing the electrophilicity of the metal center is illustrated by the lower surface in Figure 5. Increasing the Lewis acidity of the metal center will tend to stabilize all products that have additional donor bonding interactions with the metal (i.e., adduct formation, agostic interactions, the  $\eta^3$ -allyl complex). The critical transition state for dehydrogenation will also be lowered, thereby accelerating the overall reaction as observed. The overall lowering of the energy surface when the metal Lewis acidity is increased is seen in the DFT-calculated<sup>28</sup> energy surfaces for reactions of **1** and **4** (except  $\text{SiMe}_2$  is replaced by  $\text{SiH}_2$ ) with ethylene.

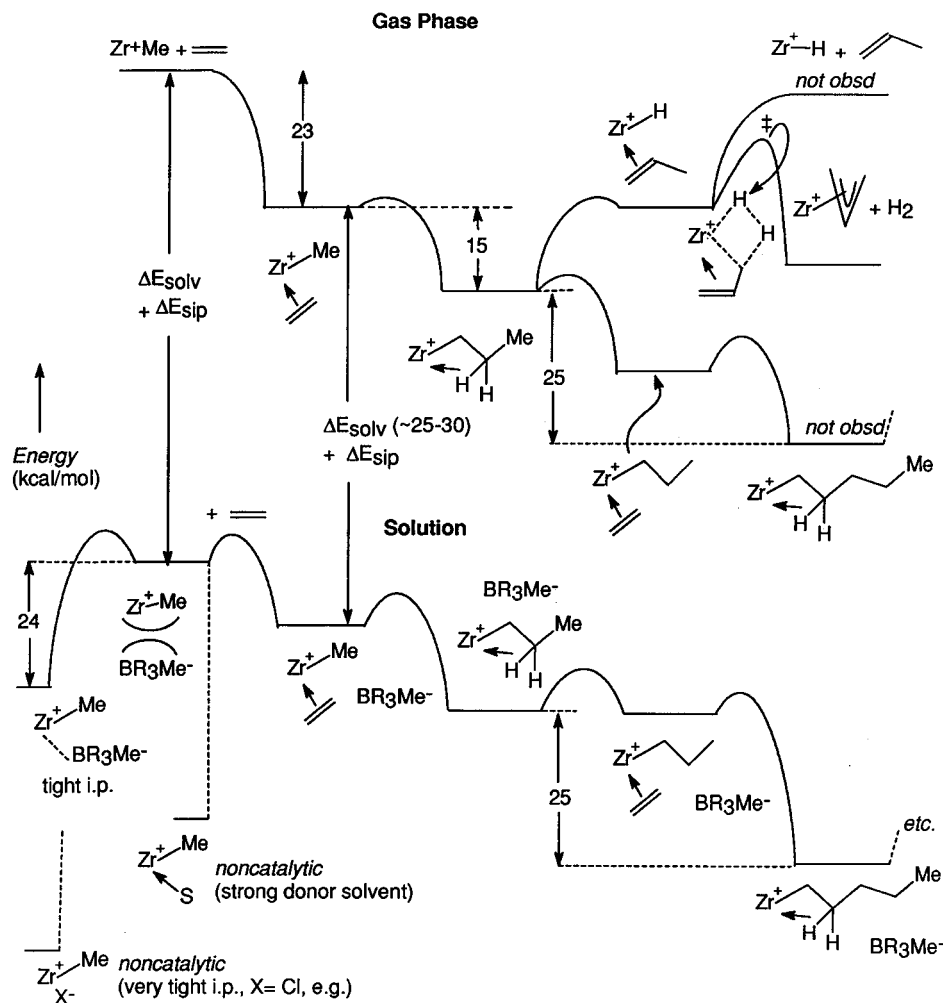
Scheme 3 illustrates the relationship between the potential energy surfaces for the gas-phase reactions and the condensed-phase reactions using ethylene as an example substrate and  $L = \text{Cp}$ . Ancillary ligands are left off the structures for simplicity. The energies shown are based on a combination of DFT,<sup>28</sup>

(28) Woo, T. K.; Fan, L.; Ziegler, T. *Organometallics* **1994**, *13*, 2252.

(29) Weiss, H.; Ehrig, M.; Ahlrichs, R. *J. Am. Chem. Soc.* **1994**, *116*, 4919.

(30) Zerner, M. C. ZINDO95 program, Quantum Theory Project, University of Florida, Gainesville, FL. See: Zerner, M. C.; Loew, G. H.; Kirchner, R. F.; Muller-Westerhoff, U. T. *J. Am. Chem. Soc.* **1980**, *102*, 589 and references therein.

Scheme 3



known thermodynamic quantities for hydrocarbons, NMR kinetic studies by Deck and Marks,<sup>12</sup> and experimental solvation energies of metallocene ions.<sup>14–17</sup> The remaining details are qualitative. The observed gas-phase reaction produces the allyl complex and dihydrogen (eq 2). Other gas-phase pathways are shown that are not observed. One of these, the elimination of propylene (i.e.,  $\beta$ -H elimination commonly observed as a termination step in solution catalysts), is not observed because the transition state for that near-thermoneutral reaction is higher than that of the observed path (dehydrogenation). Although the insertion of a second ethylene into the Zr–propyl bond is substantially exoergic and is expected to have a low barrier,<sup>28,29</sup> the bimolecular nature of the reaction means that it will not compete with the unimolecular elimination of dihydrogen.

To connect the gas-phase potential energy surface with that for solution, we introduce the solvation energies for each species along the various pathways. A borate anion with known<sup>12</sup> ion pairing energy ( $\text{MeB}(\text{C}_6\text{F}_5)^-$ ) is shown as the weakly coordinating counterion. Solvation energies for coordinatively saturated metallocenium ions are about 20–40 kcal/mol in polar solvents depending on the Cp substituents (the high end of the range would be an appropriate estimate for  $L = L' = \text{Cp}$ ).<sup>14–17</sup> For typical nonpolar solvents used in polymerization studies (e.g., toluene) the range would be expected to be  $\sim 15$ –30 kcal/mol based on application of a Born correction for the lower dielectric constant. The energy due to formation of the separated ion pair ( $\Delta E_{\text{sip}}$ ) is not known, but the energy difference between the separated and tight ion pair is estimated<sup>12a</sup> by studies of Me interchange by NMR ( $\sim 24$  kcal mol<sup>-1</sup>).

On the lower surface in Scheme 3, two situations can be illustrated that are known to reduce or effectively eliminate polymerization activity in these systems. First, tighter ion pairing will make initiation via capture of the separated ion pair by monomer improbable (shown for the limiting case of a chloride complex). Second, a strong donor solvent will lead to ion pair separation and coordination of the solvent that cannot be displaced by monomer (shown as binding by “S”). The reactivity tuning in these catalysts follows a well-established pattern in multistep catalysis,<sup>31</sup> i.e., no intermediate in an efficient catalytic process can be exceptionally lower in energy than others along the reaction coordinate.

It is noted in the present work that all reactions involving a 4-center/4-electron transition state slow as Ind and Flu are substituted for Cp. Thus, the Ind and Flu complexes are less electrophilic (for these types of reaction, to be explicit). In analyzing how this change in electrophilicity transfers to solution, one solvates the reactants and transition states and deduces the resulting reactant to transition state energy. Assuming the solvation energies are roughly constant for a given L, then the gas-phase order of electrophilicity for the reactions studied here would be found in solution as well. The key assumption of our analysis is that the effect of the ancillary ligand substitution is the same on any 4-center/4-electron transition state, including the crucial insertion of an alkene into a Zr–alkyl bond. With the same assumption about solvation as above, the conclusion is that insertion (i.e., propagation) will

(31) For biochemical catalysis, see, for example: Fersht, A. *Enzyme Structure and Mechanism*, 2nd ed.; W. H. Freeman: New York, 1985.

be slower as Cp is substituted with Ind and Flu. Thus, based on the order of electrophilicity observed in the gas-phase reactions of eqs 1–8, we suggest that the order of  $k_{\text{prop}}$  is most likely  $4 > 1 > 2 > 3 > 5$ .<sup>32</sup> If the solvation energies of all intermediates and transition states are constant for a given ancillary ligand set, the trends observed in the gas phase kinetics will also be observed in solution. We assume that steric effects specific to the insertion reaction are not significant.

**Polymerization Rate Laws.** We now consider how less electrophilic complex ions can lead to more active catalysts from the perspective of polymerization rate laws. For purposes of illustration, a simplified mechanism is shown in Scheme 4 for the solution polymerization of a 1-alkene by a cationic zirconocene catalyst. Actual initiation of the chain reaction can only occur once the solvent-separated ion pair is trapped by a monomer insertion. Propagation is terminated in this scheme by a  $\beta$ -H elimination step, and the zirconocene hydride is assumed to be rapidly deactivated. In actual catalytic systems, hydride intermediates can contribute to propagation by reacting further with monomer. (Although the rate laws would be more complex, conclusions will not be altered by including polymerization catalysis by the hydride complex.) Rate laws for the rate of overall propagation rate ( $R_p$ , which is monomer consumption rate) for the general and limiting cases are shown below.

$$R_p = \frac{-d[\text{monomer}]}{dt} = \frac{k_1 k_{\text{ini}} k_{\text{prop}} [\text{monomer}]^2 [\text{ZrMeX}]}{k_{\text{term}} (k_{-1} [\text{X}^-] + k_{\text{ini}} [\text{monomer}])} \quad (19)$$

The second-order term in monomer in the numerator arises because the initially inserted monomer ( $k_{\text{ini}}$  step) is always present in the activated complex for propagation steps (not because a second monomer is coordinated and promotes insertion). If  $k_{-1} [\text{X}^-] \gg k_{\text{ini}} [\text{monomer}]$ , then

$$R_p = \frac{K_{\text{ip}} k_{\text{ini}} k_{\text{prop}} [\text{monomer}]^2 [\text{ZrMeX}]}{k_{\text{term}} [\text{X}^-]} \quad (20)$$

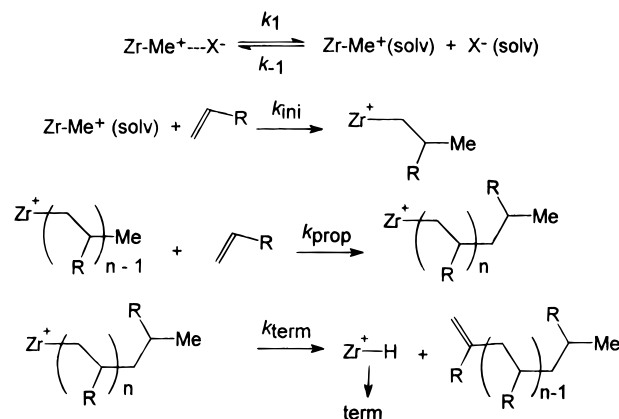
If  $k_{-1} [\text{X}^-] \ll k_{\text{ini}} [\text{monomer}]$ , then

$$R_p = \frac{k_1 k_{\text{prop}} [\text{monomer}] [\text{ZrMeX}]}{k_{\text{term}}} \quad (21)$$

Thus, observed order in monomer can range from 1 to 2. In the limiting case where  $k_{-1} [\text{X}^-] \gg k_{\text{ini}} [\text{monomer}]$ ,  $R_p$  is proportional to  $(K_{\text{ip}} k_{\text{ini}} k_{\text{prop}}) / k_{\text{term}}$ , where  $K_{\text{ip}} = k_1 / k_{-1}$ . Thus, when the reverse reactions of an ion-pairing equilibrium are much faster than reaction with monomer (i.e., rapid preequilibrium), the overall rate of polymerization depends on the equilibrium constant for ion-pair separation and the rates of initiation, propagation, and termination. Any attempt to ascertain the separate effects of modification of ancillary ligands on each of these steps by measuring overall catalyst activity will be difficult at best.

If the propagation reaction rate (controlled by  $k_{\text{prop}}$  in Scheme 4) decreases with more electron-donating ligands such as Ind, then an observed increase in the activity for the Ind catalyst must arise from changes in the ion pair equilibrium constant, initiation rate, or termination rate. A likely candidate is the ion pair binding constant. Bulkier ligands may reduce the binding constant for the counterion to the cationic catalyst and

#### Scheme 4



thereby accelerate the polymerization by increasing the equilibrium amount of the solvent-separated cation.

#### Conclusions

The following principal conclusions can be drawn from the present results:

(1) The electrophilicity of  $[\text{L}_2\text{Zr}-\text{CH}_3]^+$  ions in the gas phase is strongly dependent on the nature of the ancillary ligands L, with electrophilicity decreasing in the order  $\text{L}_2 = \text{Cp}_2 > \text{Cp}$ ,  $\text{Ind} > \text{Ind}_2 > \text{Flu}_2$  for reactions with dihydrogen and 1-alkenes. Silyl bridging of Cp ligands appears to increase the electrophilicity somewhat, and the highly electron-deficient ion **6** also has higher electrophilicity than the *bis*-Cp ion **1**. In each reaction used to assess electrophilicity, the probable rate determining transition state involves a 4-center/4-electron species in either C–H or H–H activation.

(2) In the reaction of ethylene with  $[\text{L}_2\text{Zr}-\text{CH}_3]^+$ , labeling studies show that partial-to-complete scrambling of H/D labels before elimination of dihydrogen. The extent of scrambling increases with the less electrophilic ions. A model for the intramolecular isotope effect suggests a KIE of 2.2 for the allylic C–H(D) activation step in reactions with the least electrophilic complex **3**.

(3) Isotopic labeling has shown that the C–H activation of isobutene by  $[\text{L}_2\text{Zr}-\text{CH}_3]^+$  proceeds via allylic activation only. This result is consistent with solution reactivity for these ions. For this substrate, intramolecular insertion/ $\beta$ -Me shifts are detected before elimination of methane by allylic activation.

(4) Reactions of  $[\text{L}_2\text{Zr}-\text{CH}_3]^+$  with  $\text{L}_2\text{Zr}(\text{CH}_3)_2$  and water are facile in the gas phase, and the products are analogous to side reactions in solution polymerizations catalyzed by these species.

(5) The polymerization activity of electrophilic polymerization catalysts does not necessarily correlate with the intrinsic electrophilicity of  $[\text{L}_2\text{Zr}-\text{CH}_3]^+$  species as L is varied. The ion pairing tendency of  $[\text{L}_2\text{Zr}-\text{CH}_3]^+$  in solution is a key part of the overall propagation rate, and the stability ( $K_{\text{ip}}$ ) of the ion pair for a given counterion is expected to decrease as L becomes more electron donating and larger. In addition, relative rates of propagation, initiation, and termination can be influenced by the ancillary ligand set. If the ion pair preequilibrium trends dominate, then more active catalysts can be obtained by introducing larger ancillary ligands with electron-donating substituents.

#### Experimental Section

The 3-T Fourier transform mass spectrometer used in the work presented here and the general procedure for collecting the mass spectrometric kinetic data are described elsewhere.<sup>19,20</sup> Specific procedures are described below.

(32) Note that propagation steps are represented by the right side of the energy curves in Scheme 3 (starting with the  $\text{Zr}^+$ -propyl intermediate). Although outersphere solvation energies vary with the nature of L, the overall exoergic of each insertion does not (to a first approximation).

**Overlapping Peaks and Product Distributions.** The complexes in this study lead to an isotopic envelope of nine peaks: four major, three minor, and two negligible (<0.5%). The details of this envelope are dominated by the five principal zirconium isotopes and the two carbon isotopes. The lowest mass peak, whose general formula is  $^{90}\text{-Zr}^{12}\text{C}_x^1\text{H}_y$ , is also the most abundant (about 40% of the total ion abundance). This means that unless two species have nominally the same mass, there will always be one peak unique to a species and, more importantly, this peak will be the most abundant peak in the envelope. The total ion intensity for a given complex ion is determined by calculating the theoretical isotope distribution and dividing the intensity of the lowest mass peak by its fractional abundance. The total ion intensity is calculated in this way for two reasons. First, the total is more accurate than that obtained by summing up all the observed peaks because the fractional error in the intensity of a larger peak will be smaller than for a smaller peak, and, as a practical matter, when there is only a small amount of a species the minor peaks might not show up above the noise (the three minor peaks together are about 10% of the total). Second, in the event of overlapping peaks, the two (or more) ions may be deconvoluted by starting on the low mass end, where there is always an ion due to a single species and subtracting off appropriate amounts from the heavier ions. The product distribution from isotopically labeled substrates is deconvoluted in this manner.

**Pressure Measurement.** The primary source of error in the derived rate constants is the measurement of the neutral pressures. The pressure measurements are taken from a nude ion gauge which is mounted over a diffusion pump (due to design constraints imposed by the presence of the high magnetic field) and hence the pressure reading will be lower than the pressure at the cell. As an approximation, the raw rate constants are divided by two to take into account the difference between the ion gauge and the cell and multiplied by the ion gauge sensitivity factor for each gas: 0.4 for  $\text{H}_2$ , 0.38 for  $\text{D}_2$ , 2.3 for  $\text{C}_2\text{H}_4$  and  $\text{C}_2\text{D}_4$ , 3.3 for  $\text{C}_3\text{H}_6$ , 3.6 for  $\text{C}_4\text{H}_8$ ,  $\text{C}_4\text{H}_2\text{D}_6$ , and  $\text{C}_4\text{H}_6\text{D}_2$ . Relative errors among the rate constants are smaller than the absolute errors, and rate constants within a series (for a given substrate) are comparable to each other. Error limits on rate constants are quoted with  $\pm\sigma$  from multiple kinetic determinations, often on different days. The absolute errors in derived rate constants are generally higher ( $\pm 50\%$ ) because of the substrate pressure uncertainty.

The rates for the formation of dimers (binuclear zirconium complexes) are dependent on the pressure of the complex. While the volatility of the compounds will make the pressure at the cell higher than that estimated by the factor of 2 quoted for the substrates, this effect is compensated by a (probably) larger ionization gauge sensitivity factor. To minimize this error, the vacuum chamber walls are heated at or above the temperature of the probe tip. Unfortunately, it is not

possible to get a pressure which is sufficiently high that a correction can be made by directly comparing the ionization gauge reading with an absolute pressure reading from a capacitance manometer.

**Data Reduction.** A rate constant is calculated based an experiment with 10–30 measurements and generally the results of five or more experiments are averaged together to improve statistics. The differential equations describing the kinetic system were integrated analytically, and the normalized intensities are fit to the intensities calculated from the model by using the rate constants as the fitted parameters by a non-linear least-squares approach. The iterative fitting procedure used a quasi-Newton algorithm for minimization with linear extrapolation from the tangent line to obtain the next guess for the rate constant values and forward differencing for estimates of the partial derivatives. The second-order rate constants are calculated by dividing the pseudo-first-order rate constants by the estimated substrate pressures.

Developing the model set of reactions was not straightforward due to the presence of side reactions competing for the methyl zirconocene reactant. The reaction with water to form the hydroxide ( $[\text{L}_2\text{ZrOH}^+]$ ) is significant, and ion reactants and products react with the neutral dimethyl parent complex to form dimer products (binuclear zirconium ions). To sort out the various pathways, double resonance experiments are performed. In this type of experiment, one species is continuously resonantly ejected from the ion trap and, after a reaction time, the presence or absence of product species reveals the effect of the ejected species.

**Reagents.** The  $\text{H}_2$  was purchased from Air Products (UHP grade). The  $\text{D}_2$ ,  $\text{C}_2\text{H}_4$ ,  $\text{C}_3\text{H}_6$ , and  $\text{C}_4\text{H}_8$  were purchased from Matheson (CP grade). The  $\text{C}_2\text{D}_4$  (98 atom % D) was purchased from Cambridge Isotope Laboratories.  $\text{C}_4\text{H}_2\text{D}_6$  (98.2 atom % D, Lot No. 3426-N), and  $\text{C}_4\text{H}_6\text{D}_2$  (97.7 atom % D, Lot No. 3425-N) were purchased from MSD isotopes. All substrates were used without further purification.

Metal complexes were prepared by literature methods<sup>33</sup> and purified by sublimation when possible. The precursor complex to **6** was provided by J. Petersen.<sup>22</sup>

**Acknowledgment.** This work was supported by a grant from the National Science Foundation (CHE9311614). Assistance by M. Zerner and M. Cory with the ZINDO95 calculations is gratefully acknowledged. Helpful discussions with J. Petersen are gratefully acknowledged.

JA9613872

(33) (a) Samuel, E.; Alt, H.; Hrcir, D. C.; Rausch, M. D. *J. Organomet. Chem.* **1976**, *113*, 331 (b) Samuel, E.; Rausch, M. D. *J. Am. Chem. Soc.* **1973**, *95*, 6263.